

DISPLACEMENT AND MASS TRANSFER OF CO₂/BRINE IN SANDSTONE

H. Ott^{*}, S. Berg, S. Oedai

Shell Global Solutions International BV, The Netherlands.

This paper was prepared for presentation at the International Symposium of the Society of Core Analysts held in Austin, Texas, USA 18-21 September, 2011

ABSTRACT

The displacement and fluid/fluid mass transfer between CO₂ and brine in Berea sandstone have been investigated by unsteady-state core-flood experiments combined with x-ray computed tomography. Relative permeability and capillary pressure saturation functions of primary drainage for mutually saturated fluid phases have been determined from production data and the saturation profiles by history matching and have been benchmarked against standard SCAL. The displacement stability of the CO₂/brine drainage process has been investigated by numerical modeling, and the consequences for experimental procedures and for geological storage of CO₂ are discussed. Aspects of mass transfer during drainage and imbibition that are relevant for non-equilibrated fluid phases were studied by core flooding with unsaturated CO₂ and brine phases.

INTRODUCTION

For CO₂ injection in saline aquifers the properties of the formation rock and the fluids play an important role. CO₂ and brine are immiscible fluids and hence subject to immiscible displacement. The two fluids are mutually soluble, leading to a mass transfer between the two fluid phases, with a potential impact on the displacement process in those areas where the two fluid phases are not yet equilibrated such as near the injection point and close to the flood front. The major part of the plume, however, might be subject to true immiscible displacement, and hence the pore space utilization and the extent of the plume are largely determined by relative permeability and capillary pressure saturation functions, $k_r(S_w)$ and $p_c(S_w)$, respectively. Characterization of the primary drainage process is essential for geological sequestration. The microscopic displacement efficiency (shock front height) and also the degree of gravity overrun, viscous fingering and channeling through rock heterogeneities determine how effectively the pore space is used for CO₂ storage. Shock front height, fingering and gravity overrun depend on fluid viscosity, k_r and p_c . Bypassing due to channeling and/or viscous instabilities is a concern, especially at a high viscosity ratio between the displaced and the displacing fluids i.e. CO₂ and brine. For a comprehensive analysis of the CO₂/brine displacement process we conducted unsteady-state (USS) core flood experiments in Berea sandstone. Mutually saturated and unsaturated CO₂ and brine phases were injected in the rock under realistic sequestration conditions to obtain $k_r(S_w)$ and $p_c(S_w)$ and to study the influence of mass

transfer on the primary drainage. As a reference case and for validation versus standard SCAL (Special Core Analysis), a decane/brine primary drainage experiment was conducted on the same sample. In addition, an imbibition experiment was performed where unsaturated brine was injected into rock filled with mutually saturated CO₂ and brine phases at near-residual CO₂ saturation. This study reflects the transition from residual trapping to solubility trapping and indicates the time and length scales involved.

MATERIALS AND METHODS

A cylindrical rock sample (“core”) contained in a metal sleeve with a Teflon liner is enclosed in a (x-ray transparent) carbon fiber epoxy core holder. Fluids were injected in a horizontal geometry through a distribution plate and a highly-permeable porous metal disk into the inlet face of the core. The same configuration was used at the outlet. The confinement pressure in the annulus between sleeve and core holder was set at 150 bar in order to avoid bypassing of fluids. The experimental setup is described in more detail in Berg *et al.* [1]. N-decane, CO₂ and brine were injected at a constant rate into the core via a high pressure syringe pump (ISCO). For equilibration of CO₂ with water and during CO₂ injection, the pumps were kept at 25°C and the CO₂ was heated to experimental temperature (45°C) in the injection lines. This results in a slight under-saturation of the CO₂, ensuring the injection of a single phase, and increases the total available CO₂ volume at experimental conditions. At the outlet, a constant pressure is maintained either by a dual cylinder piston pump (Quizix) or by two Tescom backpressure controllers which are operated in series. All seals were made from Teflon and Viton-A (Shore 90). Injection rates ranged between 0.25 and 0.5 ml/min which corresponds to flow velocities of 1.2 to 2.3 foot/day, i.e. typical field flow rates. The associated microscopic capillary numbers are $N_{cap} = \mu v / \sigma \approx 10^{-8} - 10^{-7}$, where μ is the viscosity of the displacing fluid, v the linear velocity, and σ the interfacial tension (for decane/brine this is 47.9 mN/m and for CO₂/brine around 30 mN/m [2-4]). The capillary numbers are well on the plateau of typical capillary desaturation curves [5].

The fluid saturations and the spatial fluid distribution in the core were determined by x-ray computed tomography using a medical CT scanner [6,7]. CT scans were performed at a spatial resolution of 0.5 mm. Fluid saturations were determined by

$$S_{CO_2} = \alpha \cdot (CT_{exp} - CT_r) , \quad (1)$$

where α is the calibration factor that relates the difference between the actual CT scan (CT_{exp}) and the reference scan (CT_r), taken at $S_W=1$, to the CO₂ saturation.

All experiments were performed in a Berea sandstone with an average porosity of 0.223 and a permeability of 380 mD. The same core was used for multiple experiments. Before each experiment, the core was cleaned with multiple pore volumes of isopropanol. After cleaning, before and after each experiment, the saturations of the core were monitored by CT scanning and the permeability was compared to the initial permeability to ensure the integrity of the core. No clay swelling or fines migration was observed. The core was

visually completely homogeneous and the porosity profile along the core, determined by CT, was homogeneous as well. Only after the contrast was maximized did the marginal bedding planes become visible in a CT cross section (dry scan), indicating a slightly more permeable middle section of the core. This minor heterogeneity, as will be shown later, has an influence on the 3D fluid saturation pattern in the core, but only very little impact on the data interpretation and the derived $k_r(S_W)$ and $p_C(S_W)$, which demonstrates that with respect to the $k_r(S_W)$ measurement, the core can be considered as homogeneous.

CO₂ is a supercritical liquid at the experimental conditions with a density of 0.41 g/cm³ [8] and viscosity of 0.033 cP at 45°C and 100 bar [9]. N-decane is a liquid with a density of 0.720 g/cm³ and viscosity of 0.75 cP at experimental conditions [10]. Brine was made from demineralized water. In order to increase the x-ray contrast between brine and the other liquids, the brine was doped with 2 wt% of CsCl. The brine viscosity is approximately 0.67 cP at experimental conditions.

PRIMARY DRAINAGE WITH SATURATED FLUID PHASES

The experiments in this study were conducted in unsteady state (USS). The sample was initially saturated with brine which was then displaced by the non-wetting phase. Two experiments were performed: the actual CO₂/brine primary drainage experiment, and, on the same rock sample, an experiment with decane as displacing phase, which allows comparison with standard SCAL experiments. In the following we focus on the CO₂/brine experiment and compare the final results with results obtained from decane/brine and with CO₂/brine literature data on the same rock type.

The core was pre-saturated with brine ($S_W=1$) that was equilibrated with CO₂. Water saturated CO₂ was injected at a rate of 0.43 ml/min (capillary number $N_{cap} \sim 1.2 \cdot 10^{-8}$) immiscibly displacing the brine at 45°C and 100 bar corresponding to reservoir conditions at about 1000 m depth. The experimental conditions are identical for all experiments in this study. Fig. 1 shows the 3D CT data during displacement, in which orange represents the CO₂ saturated volume. The initial rock/brine system is represented as semitransparent background.

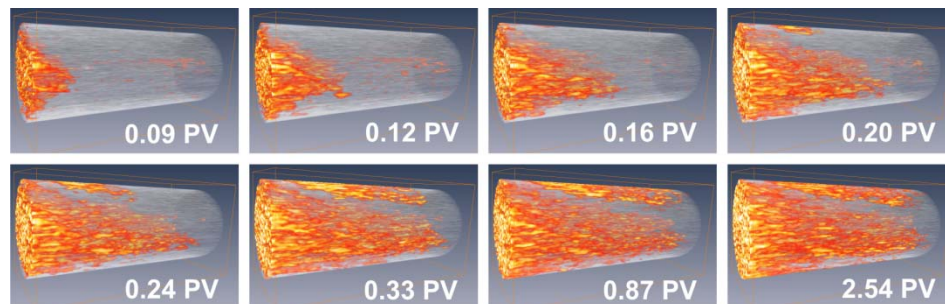


Figure 1: 3D CT data of the CO₂/brine primary drainage process in a Berea sandstone core. The images were recorded at different time steps (PV injected). CO₂ saturation is displayed in orange.

During the experiment the brine is displaced in the rock matrix and approximately half of the brine saturation remains. In contrast to the decane/brine experiment, pronounced channeling in a layer and gravity overrun of CO₂ is observed, which are responsible for the early breakthrough. The CT saturation profiles and the resulting production curve are shown in the left and right panels of Fig. 2, respectively.

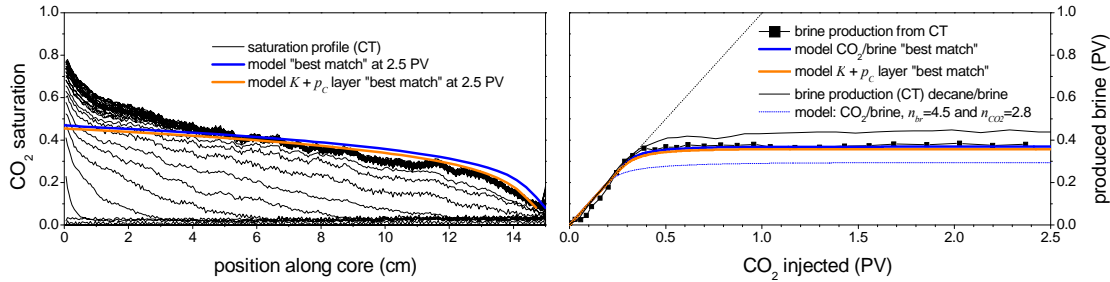


Figure 2: CO₂ saturation profiles (left) and production curve (right) during CO₂/brine primary drainage as derived from the CT scans and numerical modeling.

The conversion factor from CT numbers to saturations, α , from Eq. 1 was determined such that the production before breakthrough follows the CO₂ injection line (Fig. 2, right panel). This scaling option (α) and the high CT contrast between CO₂ and CsCl-doped brine allows a precise determination of absolute saturation with an uncertainty in the order of 2%, independent of the knowledge of the exact x-ray absorption coefficients. The data was analyzed by means of numerical simulations based on two-phase Darcy flow with a Corey representation of relative permeability. The "best match" between model and experiment was obtained by adjusting $k_r(S_w)$ and $p_c(S_w)$. The experimental data that were used for matching are mainly the CT brine production and the spatial saturation profiles $S_w(x,t)$ along the core, which are sensitive to both $k_r(S_w)$ and $p_c(S_w)$. The saturation profiles exhibit end effects at the inlet and at the outlet. The capillary end-effect [11] is typical for drainage in a water-wet core and was used to determine $p_c(S_w)$ using an initial guess for $k_r(S_w)$ from the final saturation profile. In the next step the production curve was used to refine $k_r(S_w)$. Often the results of the numerical match are not entirely consistent with all experimental data, and the resulting k_r and p_c curves are adjusted to obtain the best compromise with highest priority to match the production curve. The differential pressure (not shown) was also used for the history match but due to experimental uncertainties¹ given a lower weight in comparison to the saturation profiles and the production curve. The primary drainage $k_r(S_w)$ and $p_c(S_w)$ that best match the experiment are displayed in Fig. 3. The CO₂/brine production curve is somewhat lower than that from the decane/brine experiment, but one has to bear in mind that the CO₂/brine viscosity ratio is smaller by a factor of 24. Due to the viscosity dependency of the mobility ratio M (Eq. 2 further below), which is the non-dimensional

¹ The differential pressure (dp) was measured over the core including end pieces and flow lines, i.e. no pressure taps were used to avoid perforation of the sleeve. Note that at a low value of dp , typically encountered in this study, multiphase flow effects in the flow lines start becoming relevant. However, dp shows reasonable agreement with the history match.

scaling group for displacement, the similar production curves must result in noticeably different $k_r(S_w)$. In addition, the interfacial tension for CO₂/brine (30 mN/m [2-4]) is smaller than for decane/brine (47.9 mN/m). Therefore, the capillary pressure p_c from the decane/brine experiment (centrifuge) was scaled by a factor of 30/47.9 (Fig. 3, right panel, solid line) according to the relationship $p_{c,2} = \sigma_2 / \sigma_1 \cdot p_{c,1}$, where the indices 1 and 2 denote decane–brine and CO₂/brine respectively.

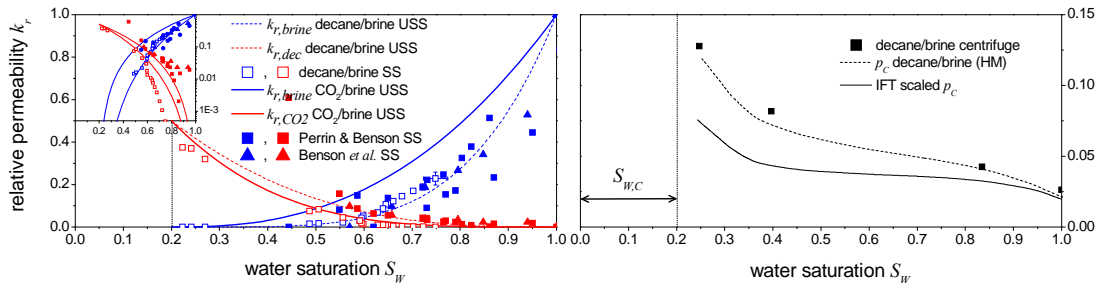


Figure 3: Primary drainage $k_r(S_w)$ (left; inset: k_r on logarithmic scaling) and $p_c(S_w)$ (right) from experiments and history matching of experimental data. Black symbols: decane/brine centrifuge data.

The CO₂/brine production curve is well described by the Corey exponents $n_{brine}=2.5$ and $n_{CO_2}=3$, which are substantially different from the decane/brine experiment from which $n_{brine}=4.5$ and $n_{decane}=2.8$ were obtained (using $S_{w,C}=0.2$, $k_{r,brine}(S_{CO_2/dec,r})=1$, $k_{r,CO_2/dec}(S_{w,C})=0.5$), and which are clearly distinguishable with an error bar of approximately $\pm 0.25^2$. CO₂/brine relative permeability data obtained by Perrin & Benson [7,12] are added to the left panel in Fig. 3 (filled symbols). The data are from steady state measurements on the same rock type (300 and 430 mD Berea samples), but show in general a substantially lower water mobility, in some cases lower than the decane/brine data. The data, measured at substantially larger capillary numbers, show unusually large residual water saturation and rather low $S_{CO_2} \approx 0.05$ for the first steady-state data point. In addition, samples used by the Benson group were fired to destroy the clays, but clays are known to play an important role in wetting effects [13].

While an overall good agreement between the production curves of the numerical model and the experiment is observed, there are some discrepancies with respect to the fluid distributions in the rock. In the experiment, at first the CO₂ predominantly flows in the middle of the rock and later gravity overrun dominates. In a homogeneous model, gravity overrun of CO₂ is the dominating mechanism at all times. Even though the permeability distribution of the rock is not exactly known, the CT scans indicate a slightly more permeable layer in the middle of the core. Therefore, a more permeable layer in the center was introduced into the model to account for the *channeling* observed in the experimental data. By channeling we mean that the displacement front is influenced by

² The error bars were determined by variation of the respective parameter keeping other parameters fixed. The sensitivity to variations of two parameters the same time was not investigated. Note that for primary drainage $k_{r,brine}(S_{CO_2,r})$ and $S_{CO_2,r}$ are already fixed, and that p_c and the absolute permeability were derived from independent experiments.

the rock structure, e.g. a variation in permeability, which is often accompanied by variation in capillary pressure. Note that channeling is different from viscous fingering, which is discussed in the next section.

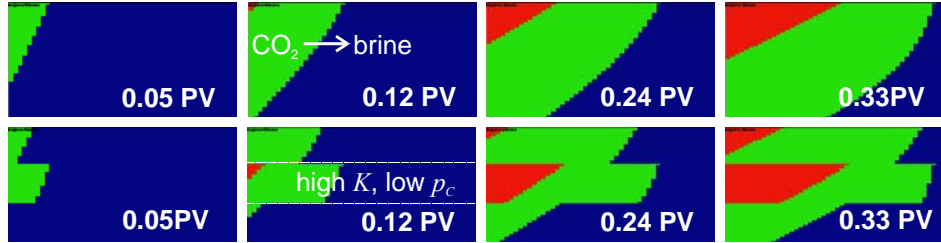


Figure 4: Results from history matching of the experimental data in Fig. 1. Upper row: simulations with a high K layer. Lower panel: including a high- K and low- p_c layer.

The spatial distribution of CO_2 from the numerical simulation with a more permeable streak in the center (upper row) and with a more permeable layer and lower p_c layer (lower row) is directly compared in Fig. 4. Permeability heterogeneity alone did not produce any channeling in the more permeable middle streak. In a modified model, the central layer was assigned a higher permeability K and a lower p_c following the principle of the Leverett- J scaling $p_c(S_w) = J(S_w)\sigma \cos\theta \sqrt{\phi/K}$, where $J(S_w)$ is the Leverett- J function specific for the rock type [5]. Keeping all other parameters constant, a larger K leads to a smaller p_c . The central layer was assigned a permeability of 420 mD while the matrix permeability remained at 380 mD. Therefore, compared to the matrix p_c , the more permeable layer has a $p_{c,high} = \sqrt{380/420}p_c \approx 0.95p_c$. In our model, we used the IFT-scaled p_c and the k_r from Fig. 3 for the matrix and lowered the p_c for the more permeable layer accordingly. The resulting production curve is added to Fig. 2. The model appears to be the best match with respect to the saturation profile, the production data *and* the spatial fluid distribution and is also compatible with the decane/brine experiment (data not shown).

VISCOUS FINGERING VS. CHANNELING

An accurate description of flood front instabilities distinguishing between channeling caused by heterogeneity and (viscous) flow front instabilities is important for accurate history matching and a correct determination of k_r and p_c . When the grid of the model is too coarse and/or (for instance) fingers are not explicitly resolved by the numerical simulation, the production curve and pressure drop of a fingering system are then described by pseudo functions which do not correctly describe the system. The advancing front observed experimentally in the center of the core (Fig. 1) could in principle also be the consequence of unstable displacement, i.e. a true instability not caused by spatial variations of rock properties.

First we clearly define the difference between fingering and channeling: while both mechanisms cause saturation patterns, channeling is the consequence of spatial variation of rock properties like permeability K , capillary pressure $p_c(S_w)$ and relative permeability

$k_r(S_W)$. Therefore, the saturation distribution can in principle be correctly described by numerical models when that spatial variation is known, e.g. by experimental measurements. Viscous fingering, in contrast, is the consequence of a hydrodynamic instability, and the condition for instability in the absence of capillarity can be derived from linear stability analysis [14]. Viscous fingering can occur even in completely homogeneous rock. Capillarity largely suppresses viscous fingering i.e. by stabilizing the flow [15]. With immiscible viscous fingering, perturbations with a wavelength λ larger than a critical wavelength λ_c can develop. The question is now whether the current situation of low-viscous CO₂ displacing brine is unstable in the sense of viscous fingering or not.

From linear stability analysis [14] the criteria for unstable displacement is the shock front mobility ratio

$$M_{SF} = \frac{k_{r,CO_2}(S_{W,SF})/\mu_{CO_2}}{k_{r,brine}(S_W=1)/\mu_{brine}} > 1 \quad (2)$$

where the mobility of CO₂ and brine are evaluated on the left and right side of the shock front, respectively. In the following consideration, the height of the shock front has been determined from a Buckley-Leverett calculation (BL) [16] for brine displacement by CO₂, ignoring capillary pressure ($p_c=0$). The resulting shock front height and the mobility ratio are shown as contours in the left and right panels of Fig. 5, respectively. The data were calculated as a function of the Corey exponents using the CO₂ and brine viscosities at experimental condition and $S_{r,CO_2}=0$, $S_{r,brine}=0.2$, $k_{r,CO_2}(S_{r,brine})=1$, $k_{r,brine}(S_{r,CO_2})=1$.

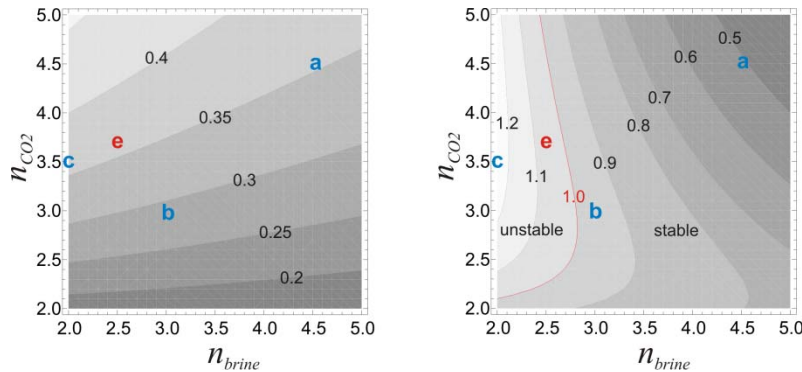


Figure 5: CO₂ shock-front height (left) and shock-front mobility ratio (right) as a function of the Corey exponents n_{brine} and n_{CO_2} . The data is calculated by BL calculation for $p_c=0$.

For the experimentally derived Corey exponents $n_{CO_2}=3.7$ and $n_{brine}=2.5$, the shock front height is 0.36, and k_{r,CO_2} at breakthrough is only 0.05. As a consequence $M=1.06$, meaning that the displacement is *marginally* unstable but it is questionable whether that would produce observable fingers on experimental scale. Note that for $n_{CO_2}=2.8$ and $n_{brine}=4.5$ from the history match of the decane/brine experiment (with $k_{r,brine}$ also representing the Perrin & Benson data – see Fig. 3), the shock-front height would be 0.24 and the

mobility ratio would be 0.73, which has direct consequences for geological storage: the shock front height and so the pore space utilization for CO₂ would be respectively lower and the travel distance of the CO₂ plume longer.

The stability criteria based on mobility ratio from Fig. 5 are confirmed by specific numerical simulations shown in Fig. 6 at an injection rate of 0.1 ml/min in a $K=100$ mD rock (with a ± 2 mD random permeability variation allowing finger nucleation), with 25% porosity and a viscosity ratio $\mu_{brine}/\mu_{CO_2} \approx 20$. Gravity effects are not taken into account.

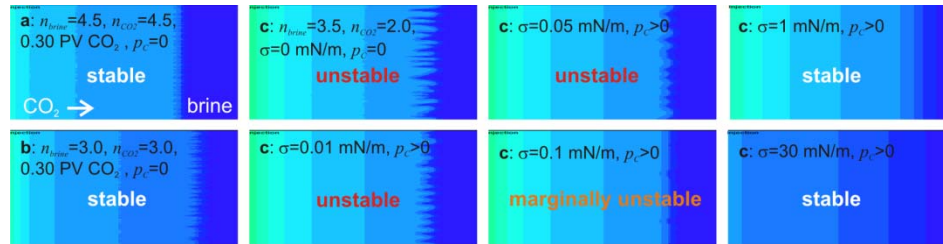


Figure 6: Numerical simulations of primary drainage in experimental geometry at different positions in the stability map (a, b, c in Fig. 5) and for different p_C levels as scaled by IFT.

For $p_C=0$ and $n_{CO_2}=4.5/n_{brine}=4.5$ (case (a) in Figs. 5 and 6) the displacement is stable in accordance with the BL calculation. There are some fluctuations at the shock front but they do not appear to grow. A similar behavior is observed in case (b) ($n_{CO_2}=3.0/n_{brine}=3.0$), which is closer to the stability limit. In case (c), $n_{CO_2}=3.5/n_{brine}=2.0$, the displacement is unstable because the fluctuations at the shock front grow into individual fingers.

The Buckley-Leverett estimates presented so far do not take capillary pressure into account but a $p_C \neq 0$ is expected to suppress fingering [15]. In order to study from which $p_C > 0$ onwards an unstable displacement turns stable, we systematically increase p_c for case (c), which is unstable for $p_C=0$. For $p_C(S_W)$ we take the decane/brine data displayed in Fig. 3 as a basis and scale them by interfacial tension σ according to $p_C = \sigma / \sigma_{decane/brine} \cdot p_{C,decane/brine}$. Unstable displacement is observed for $p_C=0$. When the interfacial tension is increased from $\sigma=0$ to 0.01 mN/m and 0.05 mN/m, the displacement remains unstable but the fingering wavelength increases qualitatively, according to linear stability analysis [14]. The situation is only marginally stable at $\sigma=0.1$ mN/m and at larger σ the displacement is stable. For the Corey parameters as extracted from the experiments and the relatively high interfacial tension between CO₂ and brine (~ 30 mN/m), we conclude that the experimentally observed saturation patterns do not originate from viscous fingering but from channeling and are hence a property of sample heterogeneity.

MASS TRANSFER DURING DISPLACEMENT

The influence of fluid/fluid mass transfer on *primary drainage* was investigated in a USS experiment on the same rock sample. Unsaturated CO₂ was injected into a rock sample pre-saturated with unsaturated brine under otherwise the same conditions. The production curves of both experiments, with mutually saturated and unsaturated fluid phases, reach very similar final plateau values as shown in the right panel in Fig. 7.

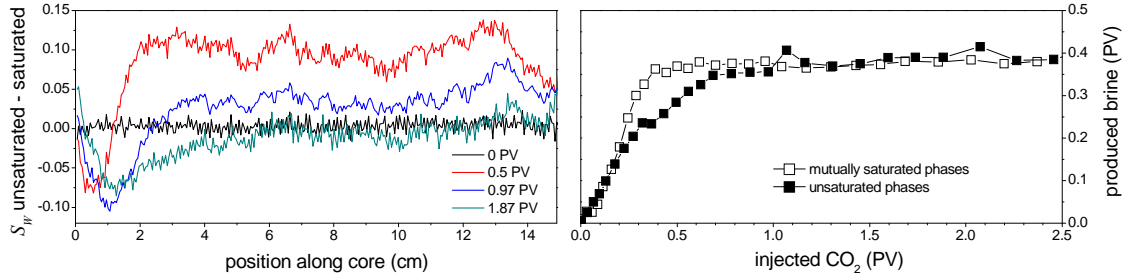


Figure 7: Brine saturation profile of the unsaturated case subtracted from the saturated case for different time steps as indicated by the injected volume (PV).

There are, however, differences in the saturation profiles between unsaturated and saturated phases. In order to directly compare the profiles for the two situations, in the left panel of Fig. 7 the differential brine saturation profiles are displayed for saturated and unsaturated experiments at the same injected PV. The dominating features are the “dip” at $x \approx 1$ cm with negative brine saturation values, and a positive offset in the differences between 0 and 1 PV injected CO₂. Negative values at the “dip” indicate a lower water saturation in the unsaturated case than in the saturated case, which is caused by evaporation of water into the CO₂ phase. The small volume of totally evaporated water of about 1 ml is compatible with the relatively small saturation limit of water in CO₂ (0.416 mol% [17-19]). Only in cases where larger amounts of CO₂ are injected is the mass balance affected [20,21]. The positive offset at 0.5 PV is a consequence of the CO₂ solubility in water which is 1.79 mol% corresponding to 9 vol% of the respective CO₂ phase [8,17-19]. For larger injected PV > 1.0 the production (and saturations) are similar in saturated and unsaturated cases (right panel of Fig. 7). But in the interval $0 \leq \text{PV injected} \leq 1.0$ the brine production of the unsaturated case falls below the production of the saturated case indicating that the brine in the core is not yet fully saturated by CO₂. As a consequence, 0.09 PV of the injected CO₂ did not displace the brine but was dissolved in it, i.e. as a first order approximation 0.09 PV less brine is produced. The offset of the profile at 0.5 PV in Fig. 7 outside of the dip is approximately 0.098 PV and compatible with the estimation from dissolution. The effect is largest at the point of breakthrough. Upon further injection of CO₂, the brine gets more and more saturated but is also increasingly displaced reaching similar saturations as in the saturated case. The first case, water dissolving in CO₂, leads to *evaporation* in a zone at the inlet, i.e. the length scale l_{evap} of water transfer at the respective flux is much smaller than the sample length. On the other hand, the solubility of CO₂ in brine influences the saturation profiles from inlet to outlet, meaning that the length scale of the effect, l_{diss} , is larger than the length of the core l_{core} and also much larger than l_{evap} , i.e. $l_{\text{diss}} > l_{\text{core}} > l_{\text{evap}}$.

To investigate mass transfer during *imbibition*, unsaturated brine was injected into the core saturated with mutually saturated brine and CO₂ at a flow rate of 0.25 ml/min. The initial state of experiment was the final state of the CO₂ drainage experiment with saturated phases but after some time in which the fluids could redistribute.

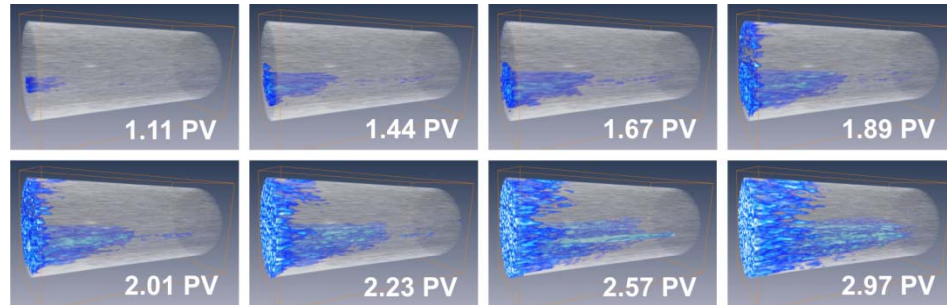


Figure 8: CT response during brine injection into CO₂/brine saturated core. An increase of brine saturation is indicated in blue, the initial rock-fluid state is semi-transparent.

Fig. 8 shows the 3D saturation patterns during brine injection with the increase of brine saturation displayed in blue. The respective saturation profiles are displayed in the left panel of Fig. 9. After the injection of about 1 PV of brine, a decrease in CO₂ saturation is visible. At this point in time Δp substantially decreases as well (data not shown) which can be interpreted as the onset of CO₂ dissolution. The increase in brine saturation causes an increase in brine k_r , and hence a decrease of the Δp .

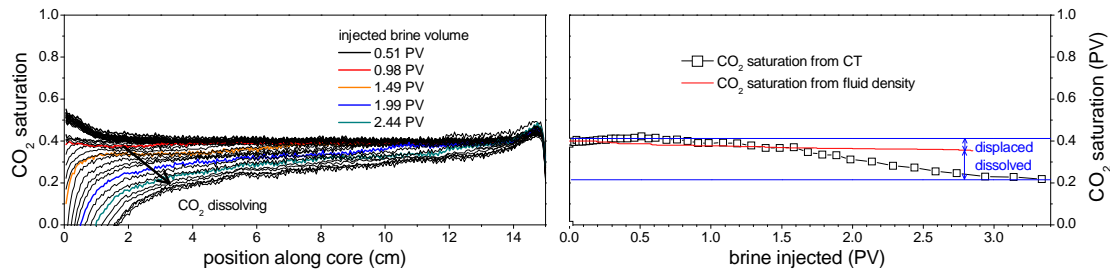


Figure 9: Imbibition of unsaturated brine in a CO₂/brine saturated core. Left: CO₂ saturation profiles for different injected brine volumes. Right: total change of CO₂ saturation.

The average CO₂ saturation in the core decreases over time as displayed in the right panel. The initial CO₂ saturation is, in principle, still mobile, i.e. subject to *immiscible displacement*. In the following we shall argue that the reduction of CO₂ saturation is caused by both the displacement and the *dissolution* of CO₂ in the injected brine, with dissolution being the dominant mechanism.

The CT data is sensitive to the total in-situ CO₂ saturation, i.e. it captures the saturation change due to displacement *and* dissolution of CO₂. The volume of the immiscibly displaced CO₂ only can be estimated from the time-integrated fluid density data (not shown). Both contributions to saturation change are compared in the right panel of Fig. 9. The difference indicates that a substantial amount of CO₂ is dissolved and subsequently miscibly displaced in the brine phase. The solubility of CO₂ in water is 1.79 mol% [8,17-

19] corresponding to 9 vol% of the respective CO₂ phase, which is substantial. Injection of 3.4 PV of unsaturated brine could dissolve 0.31 PV (48 ml) of the CO₂ phase. In the experiment, the CO₂ saturation decreases by 0.19 PV, which is of the same order of magnitude as would be expected from solubility only.

SUMMARY AND CONCLUSIONS

We performed CO₂/brine USS drainage experiments on Berea rock with a very low degree of heterogeneity. A core flood with mutually saturated fluid phases was performed to obtain relative permeability and capillary pressure saturation functions (k_r/p_C) from history matching with a homogeneous numerical model. A sensitivity test showed that the degree of heterogeneity in this sample has only very little impact on the resulting k_r/p_C , but influences the exact 3D fluid distribution in the core during the experiment. As water-wet reference and for validation against standard SCAL, a decane/brine primary drainage was performed on the same rock sample and under identical conditions. The k_r/p_C functions obtained were in good agreement with the results from steady-state and centrifuge measurements from twin samples. The CO₂/brine relative permeability was found to be different from that of decane/brine, reflecting a different wetting state. The CO₂/brine data appear to be more intermediate-wet compared to a water-wet situation for decane/brine in accordance with contact angle data from literature. The data are also different from recently published CO₂/brine data recorded on the same rock type. In particular the reported $k_{r,brine}$ is substantially lower than in the present case, which has direct consequences for the calculation of pore space utilization for CO₂ storage, for CO₂-plume migration and for determination of the stability of the flood front. The experimental data, together with a stability analysis based on a Buckley-Leverett approach and on numerical modeling, showed that the CO₂/brine displacement is stable, i.e. not subject to viscous fingering. However, due to the mobility ratio there is pronounced channeling in otherwise minor heterogeneity. Numerical modeling suggests that p_C heterogeneities rather than the related permeability variation cause channeling.

When comparing saturated with unsaturated CO₂/brine drainage experiments, solubility and mass transfer from brine to CO₂ and from CO₂ to brine were observed. The first case, water dissolving in CO₂, leads to *evaporation* at a zone at the inlet, i.e. the length scale l_{evap} of water transfer at the respective flux is much smaller than the sample length. The effect is small and negligible on an overall mass balance. The second effect, CO₂ dissolution in brine, is a relatively large effect (high solubility) and leads to a diminished displacement of brine by CO₂ which is most pronounced at the point of breakthrough. The magnitude of the effect is close to predictions from solubility data. This effect influences the saturation profiles from inlet to outlet, meaning that the length scale of the effect, l_{diss} , is larger than the length of the core l_{core} and also much larger than l_{evap} , i.e. $l_{diss} > l_{core} > l_{evap}$. Imbibition of unsaturated brine into the rock sample at near residual (trapped) CO₂ saturation shows first the miscible displacement of saturated by unsaturated brine and then a dissolution of the CO₂ phase. This experiment represents the transition from residual trapping to solubility trapping.

REFERENCES

- * Corresponding author; E-mail address: holger.ott@shell.com, research@holger-ott.de
1. Berg, S., Oedai, S., Landman, A. J., Brussee, N., Boele, M., Valdez, R., van Gelder, K., "Miscible displacement of oils by carbon disulfide in porous media: Experiments and analysis", *Phys. Fluids*, (2010) **22**, 113102.
 2. Chalbaud, C., Robin, M., Lombard, J.-M., Bertin, H., Egermann, P., "Brine/CO₂ interfacial properties and effects on CO₂ storage in deep saline aquifers", *Oil & Gas Science and Technology Rev.*, (2010) IFP **65** (4), 541–555.
 3. Hebach, A., Oberhof, A., Dahmen, N., Kögel, A., Ederer, H., Dinjus, E., "Interfacial tension at elevated pressure - measurements and correlations in the water + carbon dioxide system" *J. Chem. Eng. Data*, (2002) **47**, 1540–1546.
 4. Yang, D., Tontiwachwuthikul, P., Gu, Y., "Interfacial interactions between reservoir brine and CO₂ at high pressures and elevated temperatures", *Energy & Fuels*, (2005) **19**, 216–223.
 5. Lake, L. W., *Enhanced Oil Recovery*, Prentice Hall, (1989).
 6. Vinegar, H. J., Wellington, S. L., "Tomographic imaging of three-phase flow experiments", *Rev. Sci. Instrum.*, (1987) **58** (1), 96–107.
 7. Perrin, J.-C., Benson, S., "An experimental study on the influence of subcore scale heterogeneities on CO₂ distribution in reservoir rocks", (2010) *Transport in Porous Media*, **82**, 93–109.
 8. Span, R., Wagner, W., "A new equation of state for carbon dioxide covering the fluid region from the triple-point temperature to 1100 K at pressures up to 800 MPa", *J. Phys. Chem. Ref. Data*, (1996) **25** (6), 1509–1596.
 9. Fenghour, A., Wakeham, W. A., Vesovic, V., "The viscosity of carbon dioxide", *J. Phys. Chem. Ref. Data*, (1998) **27** (1), 31–44.
 10. Shell Global Solutions, 2008. Shell proprietary phase behavior description with a modified version of the Redich Kwong equation of state.
 11. Huang, D. D., Honarpour, M. M., "Capillary end effects in coreflood calculations", *Society of Core Analysis Conference Paper*, (1996) **SCA96-34**, 1–10.
 12. Perrin, J.-C., Krause, M., Kuo, C.-W., Miljkovic, L., Charob, E., Benson, S. M., "Core-scale experimental study of relative permeability properties of CO₂ and brine in reservoir rocks", *Energy Procedia*, (2009) **1**, 3515–3522.
 13. Anderson, W. G., "Wettability literature survey - part 1: Rock/oil/brine interactions and the effects of core handling on wettability", *Journal of Petroleum Technology*, (1986) **38**, 1125–1144.
 14. Saffman, P. G., Taylor, G. I., "The penetration of a fluid into a porous medium or hele-shaw cell containing a more viscous liquid", *Proc. Roy. Soc. London*, (1958) **Ser. A 245**, 312.
 15. Daripa, P., Pasa, G., "On capillary slowdown of viscous fingering in immiscible displacement in porous media", *Transport in Porous Media*, (2008) **75**, 1–16.
 16. Buckley, S. E., Leverett, M. C., "Mechanism of fluid displacement in sands", *Transactions of the AIME* (1942) **146**, 107–116.
 17. Marini, L., *Geological Sequestration of Carbon Dioxide: Thermodynamics, Kinetics, and Reaction Path Modeling*, Elsevier, (2007).
 18. Spycher, N., Pruess, K., Ennis-King, J., "CO₂-H₂O mixtures in the geological sequestration of CO₂. I. assessment and calculation of mutual solubilities from 12 to 100°C and up to 600 bar", *Geochim Cosmochim Acta*, (2003) **67** (16), 3015–3031.
 19. Spycher, N., Pruess, K., "CO₂-H₂O mixtures in the geological sequestration of CO₂. II. partitioning in chloride brines at 12-100°C and up to 600 bar", *Geochim Cosmochim Acta*, (2005) **69** (13), 3309–3320.
 20. Yan, W., Stenby, E. H., "The influence of CO₂ solubility in brine on CO₂ flooding simulation", *Society of Petroleum Engineers Conference Paper*, (2009) **SPE 124628**, 1–23.
 21. Ott, H., de Kloe, K., Taberner, C., Marcelis, F., Wang, Y., Makurat, A., "Rock/Fluid Interaction by Injection of Supercritical CO₂/H₂S: Investigation of Dry-zone Formation Near the Injection Well", *Society of Core Analysis Conference Paper*, (2010) **SCA2010-20**, 1–12.